Interplay of fluvial incision and rockfalls in shaping periglacial mountain gorges

Thibaut Cardinal, Laurence Audin, Yann Rolland, Stéphane Schwartz, Carole Petit, Swann Zerathe, Laurent Borgniet, Regis Braucher, Jérôme Nomade, Thierry Dumont, et al.

Interplay of fluvial incision and rockfalls in shaping periglacial mountain gorges

Thibaut Cardinal[1], Laurence Audin[2], Yann Rolland[3], Stéphane Schwartz[2], Carole Petit[1], Swann Zerathe[2], Laurent Borgniet[4], Régis Braucher[5], Jérôme Nomade[2], Thierry Dumont[2], Valery Guillou[5], and ASTER team[5,*]

Thibaut Cardinal[1], Laurence Audin[2], Yann Rolland[3], Stéphane Schwartz[2], Carole Petit[1], Swann Zerathe[2], Laurent Borgniet[4], Régis Braucher[5], Jérôme Nomade[2], Thierry Dumont[2], Valery Guillou[5], and ASTER team[5,*]

[1] Université Côte d'Azur, CNRS, Observatoire de la Côte d'Azur, IRD, Géoazur, F-06560 Valbonne, France, cardinal@geoazur-unice.fr, petit@geoazur-unice.fr

[2] Université Grenoble Alpes, Université Savoie Mont Blanc, CNRS, IRD, IFSTTAR, ISTerre, 38000 Grenoble, France, laurence.audin@ird.fr, thierry.dumont@univ-grenoble-alpes.fr, jerome.nomade@univ-grenoble-alpes.fr, stephane.schwartz@univ-grenoble-alpes.fr, swann.zerathe@ird.fr

[3] Université Savoie Mont Blanc, CNRS, Pôle Montagne, Edytem, F-73370 Le Bourget-du-Lac, France, yann.rolland@univ-smb.fr

[4] Université Grenoble Alpes, INRAE, LESSEM, F-38000, Grenoble, France laurent.borgniet@inrae.fr

[5] CEREGE, Aix-Marseille Univ., CNRS, IRD, Coll. de France, INRAE, Technopôle de l'Environnement Arbois-Méditerranée, BP80, 13545 Aix-en-Provence, France, braucher@cerege.fr, guillou@cerege.fr, bourles@cerege.fr

**ASTER Team: Georges Aumaître, Didier L. Bourlès, Karim Keddadouche*

ABSTRACT

Fluvial incision is the consequence of landscape readjustment to combined tectonic and climatic processes. In the southwestern Alps (Haute Provence Geopark), deep gorges

incised by the Bès River attest of efficient erosional processes at the front of the Alpine mountain range. This catchment stands in a peripheral Alpine position, out of the glaciated domain during the last glacial periods, which makes it suitable to quantify fluvial incision and related erosional processes in a glacier-free environment. In this paper, we combine high resolution 3D topographic mapping and in situ produced cosmogenic ^{36}Cl dating of a mountain gorge (the "Clue de Barles" Gorge). First, the very high-resolution 3D topographic modeling from aerial and drone surveys permits to map the erosion markers on the gorge walls and to accurately determine the topographic shielding factor for CRE dating. Secondly, ^{36}Cl Cosmic Ray Exposure (CRE) age distribution highlights two distinct geomorphic domains along the vertical profile: i) the higher section is characterized by clusters of similar CRE ages, interpreted as related to paraglacial rockfall events; ii) the lower section shows increasing ages with height, which are ascribed to fluvial incision occurring at a rate of 0.15 mm/yr since 25ka, and of 2 mm/yr since 2ka. Our results for the Clue de Barles, compared to other sites in the South French Alps highlight that: i) the gorge morphology is the result of the combination of both vertical fluvial incision and lateral gravitational processes, ii) the mean Quaternary fluvial incision rate in the Bès River catchment is at least twice lower than further east in the formerly glaciated Alps.

Keywords: Fluvial incision; Mountain gorge; Rockfalls; CRE ^{36}Cl dating; High-resolution 3D mapping; Southwestern Alps

1. INTRODUCTION

The erosive response of landscapes through times provides a record of the interaction between lithospheric and atmospheric forcing. The lithospheric forcing comprises isostatic readjustment and tectonic motions (England and Molnar, 1990; Lavé and Avouac, 2001; Wobus et al., 2006), while the atmospheric forcing consists of local or global climate variations (Van der Woerd et al., 2002; Pan et al., 2003; Bacon et al., 2009). Fluvial, glacial

and gravitational erosion processes play a significant role in the shaping of the landforms in an "erosion-uplift" self-balancing system (Adams, 1985). River dynamics therefore provide quantitative information on landscape evolution because their morphology and erosive power are directly linked to processes that can affect landforms: tectonic, mass movements, climate change (Pratt et al., 2002; Kirby and Whipple, 2012).

The study of fluvial landscapes evolution relies on available Quaternary geomorphological markers like terraces and incised river gorges (Pazzaglia et al., 1998; Saillard et al., 2014; Rolland et al., 2017). However, processes that led to the formation of these geomorphological objects are often poorly quantified when it comes to vertical markers. Indeed, these 3D morphologies record a combination of different mechanisms such as fluvial incision, gravitational destabilization, like landslides or rockfalls, or glacier advances related to late glacial episodes (Whipple et al., 1999; Brocklehurst and Whipple, 2002; Montgomery, 2002; Brocard, 2003; Valla et al., 2011). Quaternary geomorphological shaping of the Alpine belt and the evolution of landforms are generally explained by the alternation of glacial and inter-glacial phases, which produce significant vertical uplift after each deglaciation (Champagnac et al., 2007, 2008; Valla et al., 2010) and lead to a strong bedrock incision by the river network. The formation of peculiar fluvial markers, like bedrock gorges (named in local French language “clues” when the river runs perpendicular to the bedding), marked by deeply incised rock walls have been variously interpreted as features typical of sub-glacial incisions (Korup and Schlunegger, 2007; Montgomery and Korup, 2010) or of fluvial incision of the Late Quaternary (Saillard et al., 2014; Rolland et al., 2017; Petit et al., 2017; 2019). In all these studies, the contribution of rockfall events has never been put forward as an efficient process for the long-term shaping of mountain gorges. These investigated catchments have headwaters located in high altitude massifs, under the influence of glaciers since the Late Glacial Maximum (LGM), which led to efficient fluvial incision during deglaciation. For all

these investigated sites, the CRE data evidenced a strong relation between the onset of incision and the post-LGM deglaciation, which led these authors to propose that climatic variations are the major external factor responsible for the incision through punctual but strong glacial outburst floods during interglacials (e.g. Petit et al., 2017; Rolland et al., 2017).

In this paper, we focus on the Clue de Barles (CdB) Gorge in southwestern Alps (Southern French Alps). The site is located at the front of the subalpine fold and thrust belt, in the Bès Valley (Figure 1A), which catchment has likely been disconnected from any significant glacial influence during the LGM (Brisset et al., 2015 and references therein). This valley is currently at the boundary between the stable Alpine foreland and the actively uplifting chain, as detected by vertical GPS measurements (>0.5 mm/yr; Serpelloni et al., 2013; Nocquet et al., 2016; Sternai et al., 2019). It thus appears as a key area to determine the response of a catchment unaffected by glaciers influence and undergoing a slow uplift.

In this paper, we aim to highlight the different erosive processes that lead to the gorge formation in a fluvial-dominated catchment, based on the acquisition of a high-resolution Digital Elevation Model (DEM) of the CdB Gorge and its related environment and a high-resolution CRE dating profile of the ~100 meters high, nearly vertical gorge walls. These new data allow us to assess the relative contribution of gravitational and fluvial incision processes in the shaping of gorges along an apparently smooth profile. Finally, we compare these data with previous studies available along different catchments in the Alpine foreland after the LGM.

2. GEOLOGICAL AND GEOMORPHIC SETTING

2.1. Geological setting: The Barles erosional "half-window"

Our geomorphic target, the "Clue de Barles" (CdB Gorge), is located in the foreland of the southwestern Alps (Figure 1A). This fold-and-thrust belt has undergone tectonic shortening in Cenozoic times due to the Alpine collision (Dumont et al., 2012; Schwartz et

al., 2017). The geological structure of the region comprises the Digne nappe, made of a thick Early Jurassic limestone and marl series in the study area, which was thrust over onto the Cenozoic foreland molassic basin presently outcropping in an erosional half-window: the Barles "half-window" in the Digne Geopark (Figure 1B; Hippolyte and Dumont, 2000). At the present time, the region is still undergoing active but very slow deformation, under a compressive tectonic context (Sue et al., 2007), as shown by geodesy (Walpersdorf et al., 2018) and seismicity (Delacou et al., 2004).

In the study area, erosion due to the Bès River, a tributary of the Durance River, has participated to the formation of the erosional half-window (Figure 1B) revealing the folded and faulted sedimentary cover in the foreland beneath the Digne Nappe (Figure 1C). The formation of this erosional feature is related to tectonic uplift controlled by Pliocene crustal thickening (Schwartz et al., 2017). Thermochronological inversion modeling by Schwartz et al. (2017) showed that the onset of the half-window exhumation began at 6 Ma (with a denudation rate of ≈0.7 mm/yr). Since then, erosion, in response to the tectonic uplift (Figure 1C), has removed up to 4 km of the Digne nappe cover.

2.2. Geomorphological setting

The diversity of landscape morphologies in the Bès Valley is partly explained by differential erosion due to the strong lithological variations between marly and carbonate rich formations. Indeed, wide, smooth and open valleys shaped by landslides and gully dynamics are observed in Middle Jurassic shales locally named the "Terres Noires formation" (Figure 2A). These low relief areas are delineated by adjacent strata of much more competent Late Jurassic limestones. The Terres Noires formation is exposed in the core of anticlines while the synclines preserve Cretaceous strata, as well as Oligocene to Miocene molassic deposits unconformably lying over the Mesozoic sequence (Figures 1C). The absence of any glacial geomorphological markers, such as moraines or U-shaped valleys, precludes any significant

glacial erosion in the Bès catchment during the LGM, as also documented by studies on the maximum glacial extension in the SW Alps (Brisset et al., 2015 and references therein). Recent incision of the Late Jurassic limestones (up to 250m thick) by the Bès River has shaped the CdB Gorge in the southern flank of the overturned "Grande Cloche" anticline (GCa; Figure 1C and 2A).

Figure 2 presents three different domains along the gorge perpendicular profile:

1) sub-horizontal surfaces above the gorge,

2) steep slopes of the two gorge walls facing each other that are widening as the altitude increases, reaching ≈ 150 m of width at ≈ 150 m high above the river level,

3) sub-vertical river polished walls that form a narrow incision canyon in the lowest part (≈ 10 m high) (figure 2B, C and D).

The V-shaped profile of the gorge suggests that at larger scale its morphology may not only be controlled by fluvial incision, but also by lateral erosional processes affecting the gorge walls as the Bès River incises vertically.

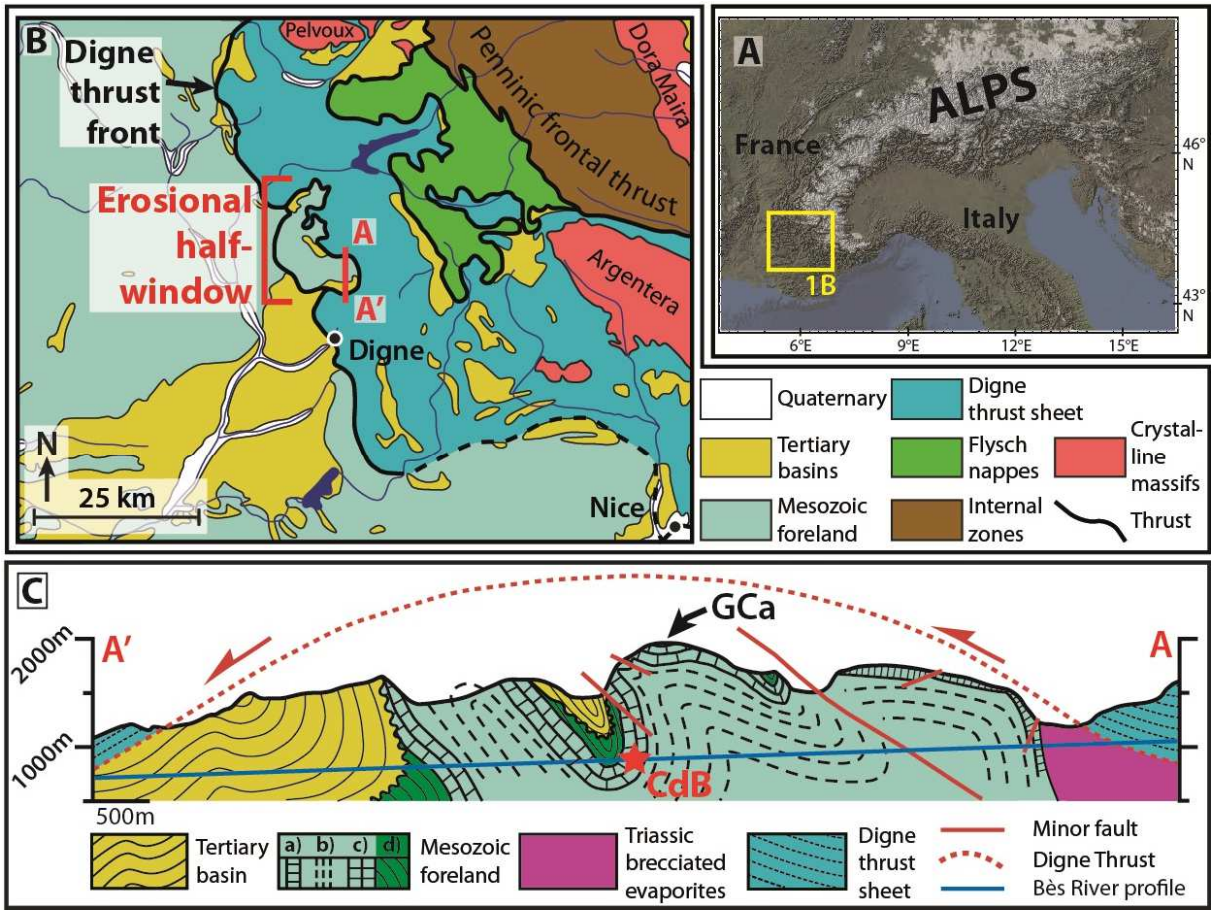

140

141 Figure 1. A, Location of study area in the European Alps. B, Location of the Barles half-window in the Western
142 Alps general tectonic framework (modified from Schwartz et al., 2017). C, Geological cross-section of the
143 Barles erosional half-window along the Bès River profile. Mesozoic foreland a) massive Early Jurassic; b)
144 Middle to Late Jurassic "Terres Noires"; c) Late Jurassic "Tithonian limestones"; d) Cretaceous. Note the
145 folding of the Tithonian limestones that form the Grande Cloche anticline (GCa) in which the Clue de Barles
146 Gorges (red star ; CdB) is dug by the Bès River.

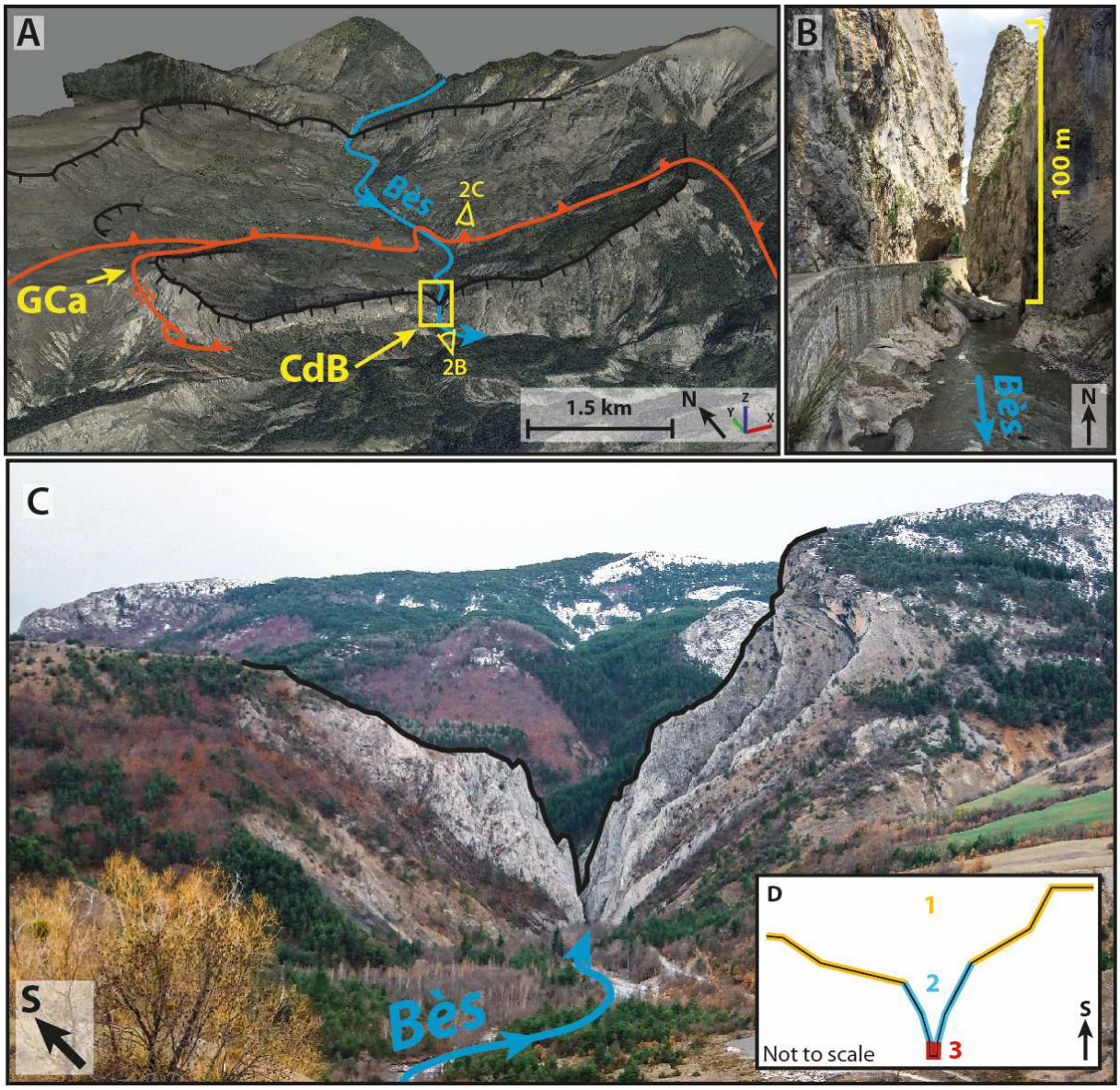

Figure 2. A, Digital Elevation Model (DEM) based 3D view from the of the study area featuring the incised limestone bars (thick black lines) north and south of a large open valley. B, Terrestrial photographs of the Clue de Barles (CdB) Gorge. C, Panoramic view of the CdB Gorge towards the South featuring the vertical Tithonian limestone strata. Note the V shaped lateral profile of the gorge, highlighted on the photographs (black thick line). D, schematic interpretation of the V shaped profile of the gorge showing the 3 different domains: 1) sub-horizontal surfaces above the gorge, 2) steep slopes of the two gorge walls facing each other that are widening as the altitude increases, reaching ≈ 150 m of width at ≈ 150 m high above the river level, 3) sub-vertical river polished walls that form a narrow incision in the lowest part (≈ 10 m high)

3. METHODS

3.1. Strategy and sampling

158 Gorge walls are theoretically gradually exposed during the incision process (Schaller et
159 al., 2005; Ouimet et al., 2008). Therefore, cosmogenic radionuclide exposure (CRE) dating of
160 the gorge wall should reveal a systematic rejuvenation of the CRE ages towards the current
161 riverbed level trough a correlation between the altitude of the samples and their CRE age.
162 However, gravitational processes, like rockfall events, may also cause the rejuvenation of a
163 gorge wall surface. If the wall compartment involved in a rockfall event is thicker than ≈ 2m,
164 the resulting exposed surface should not retain any cosmogenic inheritance prior to the
165 gravitational event, as ≈ 95% of the cosmic radiation is absorbed in the first 1.8 m below the
166 surface (Lal, 1991). Hence its concentration in cosmogenic nuclides should be null at the time
167 of the rockfall, and subsequently, the CRE age should correspond to that of the gravitational
168 event. Therefore, cosmogenic radionuclide concentration measurement is a well suited dating
169 method to obtain chronological information of both gravitational and fluviatile processes, and
170 thus allows dating rockfall events and quantifying incision rate on the same spot.
171 Sampled surfaces were chosen for incision rate estimation, based on the following
172 morphological indices: i) a surface with evidence of induration varnish or with low apparent
173 superficial dissolution, indicating little erosion since exposure or ii) vicinity to peculiar
174 concave erosional surfaces ("pot holes") preserved in the gorge walls that points to the last
175 stalling point before the incision phase. The identification of such markers and the necessity
176 to avoid samples with a too large topographic shielding led to the choice of a ≈10 m high,
177 well-preserved wall located at the southern (i.e., downstream) extremity of the gorge (Figure
178 3). The dissolution, weathering patina and superficial smoothing of the limestone surface of
179 the gorge prevented us from confidently identifying a priori gravitational markers from the
180 wall morphology through field and DEM based observations, by any rockfall scars
181 characterized by edged surface and distinct coloration due to the lack of patina. We then
182 chose to sample regularly the ≈ 70 m high wall rising above the preserved surface along a

183 sub-vertical profile (Figure 3A and 3C).

184 Along this profile, twenty limestone samples were collected, using a drill, hammer and
185 chisel. The sampled surfaces include the lower and preserved river-polished surface and the
186 upper slightly widening part of the gorge wall. In total, the gorge profile extends from the
187 river up to 80 m high on two parallel vertical limestone strata (Figure 3C). We sampled
188 surfaces with no overhanging relief to minimize the topographic shielding and to simplify the
189 topographic shielding factor determination.

190 In parallel, four samples were collected on the eastern sub-horizontal top of the limestone
191 bar overlooking the gorge to constrain the local denudation rate in this part of the catchment
192 (Figure 2C and 3A)

193 **3.2. Analytical protocol**

194 Samples were prepared at the Laboratoire National des Nucléides Cosmogéniques
195 (LN2C; CEREGE, Aix-en-Provence) following the procedure presented by Schimmelpfennig
196 et al. (2009). ^{36}Cl concentrations were determined by accelerator mass spectrometry (AMS)
197 performed on ASTER, the French national AMS facility (CEREGE, Aix en Provence)
198 (Arnold et al., 2010). All measurements were calibrated against in-House CEREGE SM-CL-
199 12 standard (Merchel et al. 2011). Total uncertainties account for counting statistics, standard
200 evolution during measurements, standard uncertainty and external uncertainties of 2.74%,
201 2.13% and 1.62 % for $^{36}Cl/^{35}Cl$, 36Cl/37Cl and $^{35}Cl/^{37}Cl$ ratios, respectively (Braucher et al.,
202 2018). The full chemical compositions of the two sampled Tithonian limestone strata were
203 analyzed at CRPG (Nancy) in order to take into account for the various ^{36}Cl production
204 pathways (Schimmelpfennig et al., 2009). A sea level and high latitude ^{36}Cl production rate
205 for calcium spallation of 42.2±3.4 atoms $^{36}Cl\ g^{-1}\ yr^{-1}$ (Schimmelpfennig et al., 2009; Braucher
206 et al., 2011) has been used and scaled after Stone (2000) and corrected for topographic
207 shielding (see next paragraph). ^{36}Cl ages have been determined using the approach of

208 Schimmelpfennig et al. (2009) using a limestone density of 2.6 g.cm^{-3}. CRE data are
209 displayed in Table 1.

210 Topographic shielding was first determined from field data. Furthermore, we chose to
211 use a high resolution DEM, built from a drone survey of the gorge and its surroundings, in
212 order to be able to precisely recalculate the shielding parameters on each sampled surface.

213 **3.3. Topographic shielding estimation in a narrow gorge**

214 The estimation of topographic shielding (TS) allows the calibration of the sampled
215 surfaces exposure ages by evaluating how much cosmic rays were obstructed by the
216 surrounding topography, which decreases the cosmogenic nuclides production rate (Dunne et
217 al., 1999). The TS factor is defined as the ratio of the received cosmic flux at a given point
218 over the maximum flux at this point assuming an unshielded exposure (Dunne et al. 1999;
219 Gosse and Phillips 2001). It is commonly calculated using the following equation from Dunne
220 et al. (1999):

221 $$C_T = 1 - \frac{1}{2\pi}\sum_{i=1}^{n} \Delta\emptyset_i \, sin^{m+1}(\theta_i)$$

222 Where C_T is the TS factor, n is the number of topographic obstructions that are measured
223 around a sampled surface, each obstruction being represented by a pair of azimuth $\emptyset_i$ and
224 elevation angles θ_i, m is a constant which commonly cited value is 2.3 (Gosse and Phillips
225 2001). This factor is commonly estimated in the field during surface sampling by measuring,
226 using a compass, the horizon elevation at 360° around the sampled surface (Gosse and
227 Phillips, 2001). However, such protocol is difficult to implement in gorges while sampling the
228 vertical wall, and is complexified by the 3D geometry of the gorge.

229 Numerical methods exist to estimate TS from Digital Elevation Models (DEM), which
230 have been demonstrated on basin-averaged denudation rate studies (e.g. Codilean, 2006;
231 Balco et al., 2008). In this paper, we used the tools developed by Li (2013), for the GIS
232 software ArcGis, using high-resolution DEMs of the CdB Gorge and its surrounding. The

DEM used are built from the Structure-from-Motion method, using aerial photographs acquired by plane, for the surrounding gorge topography, and UAV, for the mapping of the vertical parts (gorges walls), following an adaptation of the methodology presented in Vasquez-Tarrio et al. (2017).

The resulting data set has a resolution of 50 cm (precision RMSE of 2.6m), for the model surroundings used for the TS factor determination, and 7cm with a precision of 16.8 cm (RMSE) for the DEM used for the mapping of the incision markers in the gorge. Such precision has been achieved in a vertical environment, such as the CdB Gorge without GPS signal, with the use of a total station (Leica TS02) for the acquisition of Ground Control Point (GCP). The code by Li (2018) allows us to calculate the maximum elevation for each azimuth value (horizontal angle from 0° to 360° by 5° increment) around the sampled surface.

In a previous study, Norton and Vanacker (2009) mentioned that the use of a DEM with resolution lower than 5 m (5 m being the optimal resolution) can cause an overestimation of the TS factor, because of the ability of cosmic rays to pass through small obstructions without any significant interaction (Norton and Vanacker, 2009). However, in gorges, the use of a higher resolution DEM is required for the numerical determination of the TS factor, as the samples were all gathered in a narrow horizontal (XY) space, even if they lie at a larger distance from each other in the vertical Z dimension. Furthermore, the only obstructions in the gorge are the ≈200 m thick limestone walls. A precise estimate of TS is very important in the CdB Gorge, as it has a large impact on the calculated CRE ages.

3.4. Denudation rates

Denudation, which includes mechanical and chemical erosion, is an important process in the shaping of carbonate landscapes (Ryb et al., 2014a; 2014b). The efficiency of the denudation process is controlled in part by the slope and convexity of the surfaces that are involved (Godard et al., 2016; Thomas et al., 2017). Gravitational processes must be

considered, but also the spatial variability of the carbonate dissolution efficiency, which results from numerous slope morphological irregularities (overhangs, recesses, fractures). Because the radionuclide concentration at the surface results from a constant competition between surface denudation and production by exposure to cosmic rays, the denudation rate is an important factor that needs to be determined in order to calculate the CRE ages. In the SW Alps, a regional denudation rate of ≈30 mm/kyr has been estimated in the literature (e.g. Godard et al., 2016; 2020; Thomas et al., 2017), and this parameter has also been constrained locally for our site by using steady-state radionuclide concentrations. For this purpose, four sub-horizontal surfaces have been sampled on the top of the limestone bar in which the gorge was incised (≈ 250 m above riverbed) (Figure 2C and 3A). The denudation rates are calculated assuming a steady-state between radionuclide production and denudation, after the procedure described Schimmelpfennig et al. (2009).

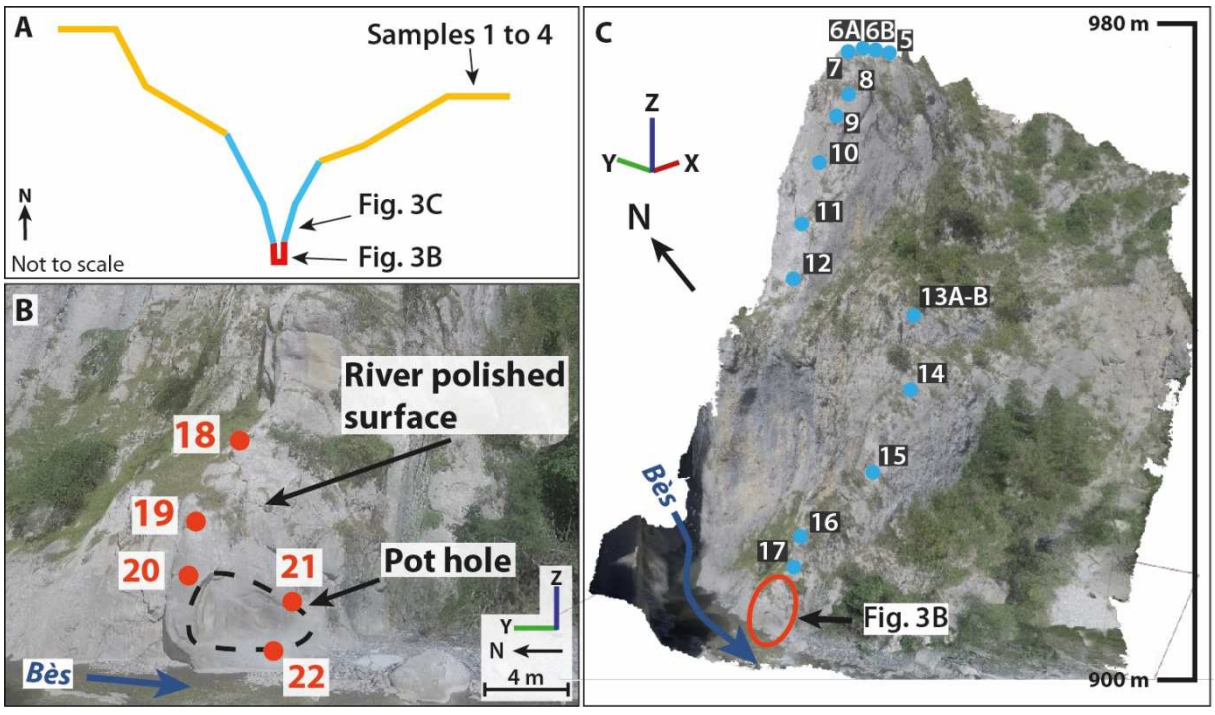

Figure 3. A, schematic interpretation of the gorge V shaped profile and location of the sample gathered for CRE dating. B, Digital Elevation Model (DEM) based 3D view of the lower part of the sampling profile and location of the corresponding samples (18 to 20). Note the presence of a "pot hole" that indicates the preserved nature of the river polished sampled surface. Above sample 18, the preservation of the fluvial polished surface on the

gorge wall is not sure and might have suffer post-incision erosion processes (dissolution and/or gravitational processes). C, All samples located on the high-resolution 3D DEM of the 80 m high CdB Gorge wall.

4. RESULTS

4.1. Flat upper surface: steady-state denudation rates

Measured radionuclide concentrations (samples 1 to 4, Figure 2C and 3A, ≈250m above river) for the horizontal high hanging paleo surfaces of the limestone bar range from 1.56 to 2.84×10^6 ^{36}Cl at/g (Table 1). Assuming these samples at steady state (i.e. their exposure time is long enough to ensure that concentrations have reach a plateau), yields to steady-state denudation rates ranging between 18.74 ± 1.05 and 32.54 ± 1.76 mm/ka for these top samples. These values are in agreement with previous estimates (e.g. Godard et al., 2016; 2020; Thomas et al., 2017, Siame et al., 2004; Zerathe et al., 2013), for the SW Alps.

4.2.Gorge steep slope / middle part: rockfall markers

4.2.1. Fracturation

The CdB Gorge walls are heavily fractured and prone to rock mass movements, as observed by our field structural analysis: two major fracture families have been measured on the gorge walls, both trending N30°E (i.e., parallel to the gorge strike), the first one dipping ~70°W and the second one dipping 40-50°E, while the bedding is ~EW and vertical (Figure 4).

4.2.2. CRE age

Denudation rates obtained on horizontal surfaces do not reflect the true denudation that has affected the vertical walls of the gorge. Indeed, it is generally considered that vertical and sub-vertical surfaces undergo less dissolution than gently dipping or horizontal surfaces, as they receive much less water runoff, and water does not stagnate or percolate (Sadier et al., 2012). Compiling denudations rates determined from our data and those from literature, we have decided to consider a denudation rate of 10 mm/ka for vertical or sub-vertical surfaces, following Sadier et al. (2012). CRE ages determined from the ^{36}Cl concentrations are reported

in the age-elevation plots (Figure 5A). The profile displays ages between 22 and 8 ka We can observe two ages clusters, one at ≈17 ka (samples 5 to 9) and the other one at ≈10 ka (samples 10 to 13A), respectively.

As shown on Figure 5A, the CRE ages distribution does not correlate with the altitude of the samples and especially, we do not see any systematic rejuvenation of the CRE ages towards the base of the gorge at the current riverbed level, as it would be expected for a gorge slope affected by post-incision erosion processes (such as rockfall or dissolution). The interpretation of these ages therefore requires a more detailed analysis taking into account the 3D morphology of the gorge walls, and the processes that may have affected the history of their exposure to cosmic rays.

4.3.River polished vertical surface / lower part: fluvial incision

CRE ages determined from the ^{36}Cl concentrations in the gorge lower part are reported in the age-elevation plots (Figure 5B). The five samples (18 to 22) display ages between 25 ka and 800 a (Table 1). From these ages, we can compute two distinct incision rates: 0.15 mm/yr from 25 ka to 2 ka and 1.97 mm/yr from 2 ka to present day, assuming a y-intercept equal to zero.

Sample	Altitude above sea level (m)	Height above river (m)	Lat	Long	Spall. scaling	35Cl (ppm)	Ca (%)	Atoms ^{36}Cl (at/g)	Atoms ^{36}Cl uncertainty (at/g)	CRE age (yr)	Denudation rate (mm/ka)	TS factor	Surface strike and dip
1	1165.0	263.0	44.23	6.26	2.64	60.5	36.0	18885474	111338	-	32.83 ± 1.94	0.99	Sub-horizontal
2	1155.6	253.6	44.23	6.26	2.62	48.5	39.0	2767824	155686	-	18.74 ± 1.05	0.99	Sub-horizontal
3	1151.7	249.7	44.23	6.26	2.61	81.3	38.2	2844314	195423	-	22.91 ± 1.57	0.99	Sub-horizontal
4	1154.9	252.9	44.23	6.26	2.62	38.0	31.9	1563115	84417	-	32.54 ± 1.76	0.99	Sub-horizontal
5	975.2	73.2	44.23	6.26	2.27	29.1	32.1	414312	21132	13598 ± 694	-	0.85	N118E23
6A	975.7	73.7	44.23	6.26	2.27	17.2	24.7	463710	20942	19805 ± 894	-	0.87	N22E4
6B	975.5	73.5	44.23	6.26	2.27	102.8	27.6	840309	279136	19240 ± 6391	-	0.87	N21W12
7	975.1	73.1	44.23	6.26	2.27	20.6	38.9	518890	23489	15334 ± 694	-	0.87	N171W33
8	969.3	67.3	44.23	6.26	2.26	32.6	32.2	397913	24537	15229 ± 639	-	0.72	N151W37
9	966.8	64.8	44.23	6.26	2.25	17.5	38.2	451597	21698	15810 ± 760	-	0.76	N170W68
10	959.8	57.8	44.23	6.26	2.24	23.6	37.2	321967	15754	9877 ± 483	-	0.84	N145W72
11	950.7	48.7	44.23	6.26	2.22	23.5	38.6	310801	16034	9791 ± 505	-	0.80	N77W72
12	944.0	42.0	44.23	6.26	2.21	22.3	37.4	298013	15522	11668 ± 608	-	0.67	N14W72
13A	940.4	38.4	44.23	6.26	2.21	28.0	38.0	290021	15713	10276 ± 556	-	0.71	N106W87
13B	940.4	38.4	44.23	6.26	2.21	43.3	38.4	257546	22005	8397 ± 717	-	0.71	N106W87
14	930.9	28.9	44.23	6.26	2.19	29.8	37.3	467713	23683	19233 ± 974	-	0.65	N140E89
15	922.4	20.4	44.23	6.26	2.17	25.3	37.3	330443	16938	16245 ± 833	-	0.55	N4E84
16	915.4	13.4	44.23	6.26	2.16	27.3	31.8	341914	17288	22348 ± 1130	-	0.47	N162W26
17	911.6	9.6	44.23	6.26	2.16	22.9	37.7	229307	13073	13660 ± 779	-	0.45	N13W71
18	908.2	6.2	44.23	6.26	2.15	29.0	38.0	396966	22406	25803 ± 1456	-	0.43	N140W80
19	907.2	5.2	44.23	6.26	2.15	30.4	35.7	268197	14974	18429 ± 1029	-	0.40	N179W61
20	905.4	3.4	44.23	6.26	2.14	28.8	33.2	98729	8562	6581 ± 572	-	0.41	N0E84
21	904.5	2.5	44.23	6.26	1.49	21.2	37.5	26219	3368	1267 ± 163	-	0.52	N155E83
22	903.6	1.6	44.23	6.26	1.49	22.6	37.4	17964	3489	830 ± 161	-	0.53	N150E56

317

318 Table 1. ^{36}Cl CRE sample characteristics and geochronological data. Sample field information, natural chlorine, calcium, and cosmogenic ^{36}Cl contents in the limestone

319 samples and resulting ^{36}Cl CRE ages and denudation rates, TS factor and strike and dip of the sampled surfaces are indicated.

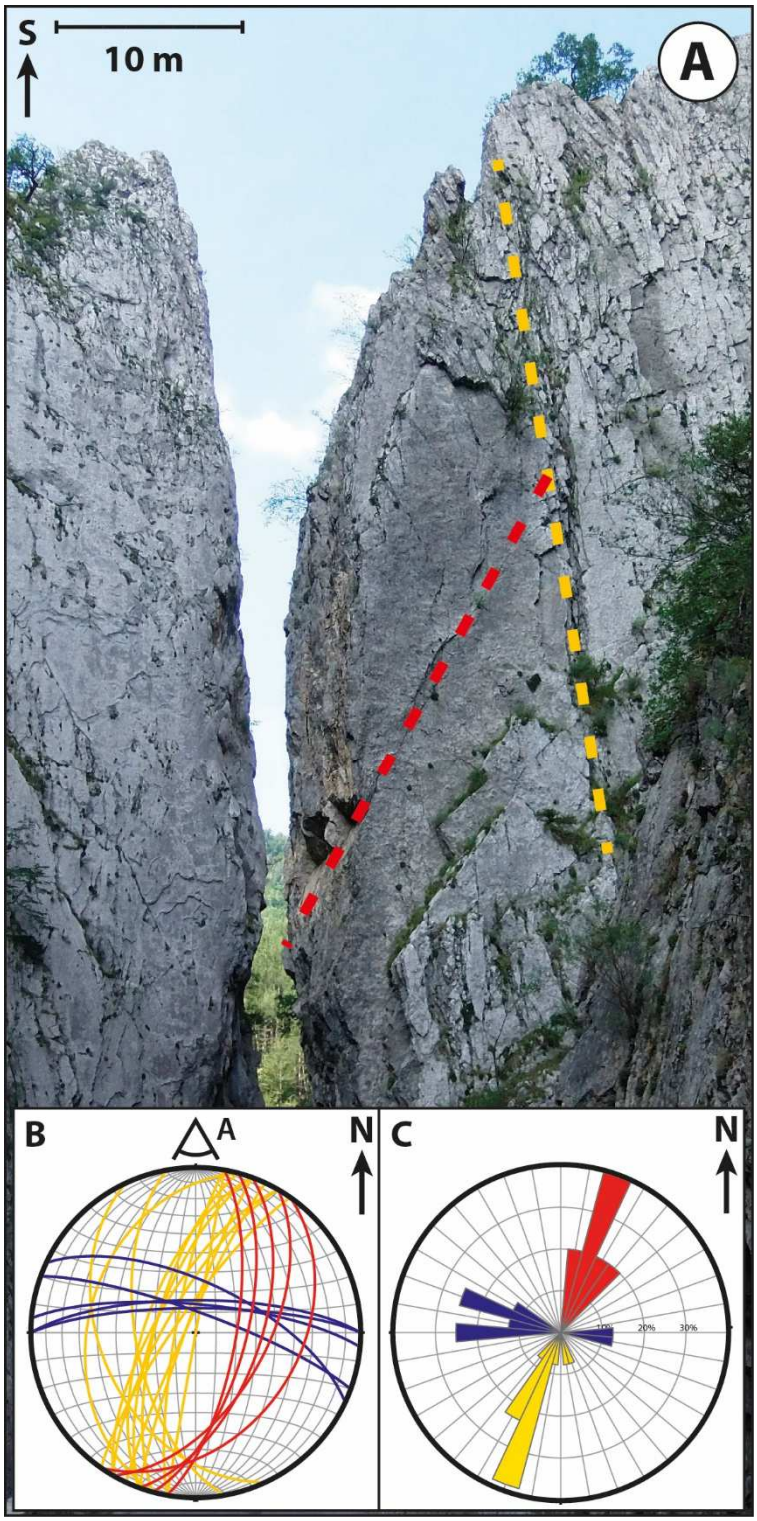

Figure 4. A, West flank of CdB Gorge viewed towards the south with the two major representative fracture planes highlighted by red and yellow dashed lines. B, Projection of bedding plane (in blue), major fracture planes visible in A (red and yellow), Wulff projection, lower hemisphere. C, Rose diagram of bedding and fracture planes (same colors).

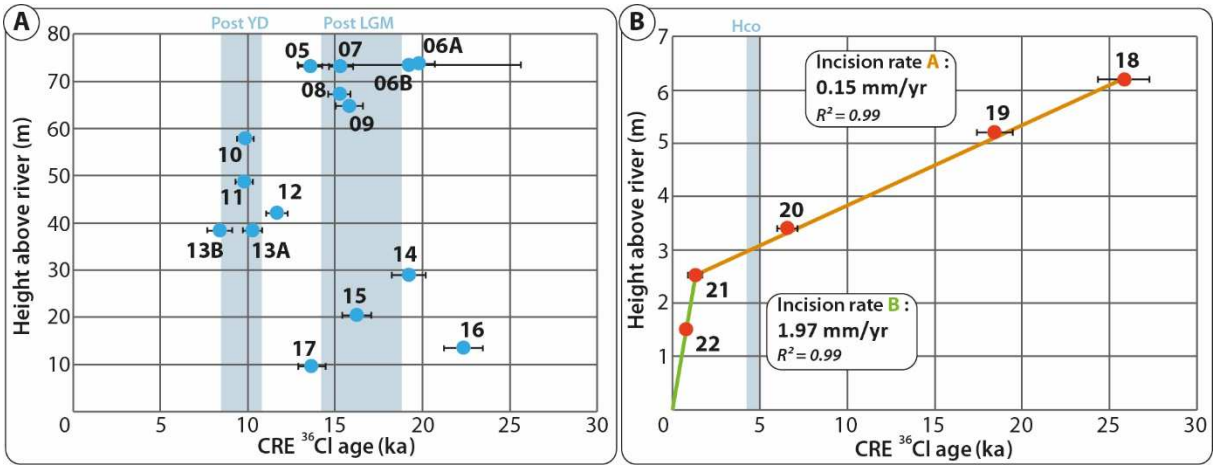

Figure 5. Height above river bed versus exposure age, determined by ^{36}Cl concentration, for the 18 dated samples collected in the middle (A) and lower part (B) of the CdB Gorge. The dot colors are in reference to the Figure 3: the red dots refer to the river polished lower part, and the blue dots refer to the middle part of profile. With the five CRE ages ascribed to the fluvial incision process (B), we are able to compute incision rates ranging from 0.15 mm/yr to 1.97 mm/yr, which might suggest an acceleration of incision after 2 ka. Known deglaciation periods are chronologically represented by light blue columns: post LGM (Last Glacial Maximum): ≈ 19-14 ka Clark et al. (2009); Post YD (Post Younger Dryas): ≈ 11-8 ka. Darnault et al. (2012); Hco (Holocene climatic optimum): ≈ 5-4 ka; Zerathe et al. (2014).

5. DISCUSSION

5.1. Geomorphological interpretation of the CRE ages

Field and DEM observations evidence that the CdB Gorge walls have been rejuvenated several times in the middle part of the sampling profile (samples 5 to 17).

Actually, detailed field structural investigations of the gorge (Figure 4) and DEM-based morphological analysis of the sampled wall (Figure 6A, B, C) attest of such gravitational processes in the CdB Gorge. All the planes (fractures and bedding) described in previous section 4.2. (Figure 4) can play a role in the occurrence of rockfall events by isolating polygonal blocks susceptible to fall from the rock scarp. Furthermore, differential erosion between the various vertical limestone strata of different thickness, ranging from ≈ 20m to > 1m, destabilizes the vertical walls and thus leads more competent strata to be in an unstable overhanging position. These observations highlight the predisposing factors and vulnerability

346 of the gorge to rockfall hazard. The combination of vertical incision and lateral gravitational
347 processes can therefore explain the peculiar V-profile of the CdB Gorge.

348 The main fracture orientations (yellow; Figure 4 and 6A, B, C), are parallel to the surface
349 of the profile in its middle part (from samples 07 to 12; Figure 6C) suggesting that this
350 surface may result from rockfall events. The fracture pattern and the morphology of the wall
351 suggest the toppling of a large vertical column (≈ 20 m high; Figure 6D), prepared by joints
352 opened within the vertical limestone beds. Following this observation and the CRE ages, it
353 appears that the column was toppled by two distinct events, involving first the upper part of
354 the column (samples 7 to 9) and then its lower part (samples 10 to 12) at ≈17 ka and ≈10 ka
355 respectively (Figure 5). Other sampled surfaces, from samples 5 to 6B and 13A to 17, show
356 an age distribution with three clusters ranging from 14.5 to 22 ka, from 10 to 30m above
357 riverbed. The age versus height distribution does not show any clear trend, which suggests
358 that these surfaces were later rejuvenated by gravitational processes.

359 Finally, in the lower part of the profile, the linear decrease of CRE ages towards the
360 riverbed is suggestive of fluvial incision, which can be separated into two phases: i) from
361 sample 18 to 21 (0.15 mm/yr), and ii) from sample 21 to riverbed (2.15 mm/yr). However, the
362 latter incision rate only concerns the foot of the gorge wall (>2.5m high) which can be
363 rejuvenated by punctual and recent flood events, and is constrained by only two points (three
364 of we take into account the (0,0) point corresponding to the river bed). Hence, the estimated
365 incision rate of 2.15 mm/yr is not representative of the long-term fluviatile incision process
366 that is responsible for the formation of the CdB Gorge.

367 **5.2. Climatic control on gravitational events**

368 Major rockfall events can be interpreted as the result of changing climate conditions,
369 as these processes are well known to be sensitive to permafrost degradation during warming
370 phases (e.g. Ravanel et al., 2010; Hilger et al., 2021). Based on our case example, these

gravitational processes appear to be an important factor of the gorge erosion process. We obtained two age clusters which we interpret as two instantaneous rockfall events having occurred at ≈17 and ≈10 ka respectively. These ages correspond to the two last major deglaciation phases: post LGM (≈ 19-14 ka; Clark et al., 2009) and post Younger Dryas (≈ 11-8 ka; Darnault et al., 2012) (Figure 5). Although reconstructions of permafrost are still lacking for this period of time, we suggest that this relatively high-altitude area could have been under permafrost influence, due to its elevation above the equilibrium line altitude for glaciers during the LGM and Younger Dryas, and its proximity to the glacier front (Brisset et al., 2015 and references therein). Therefore, these gravitational events could have been caused by permafrost degradation, adding to a potential increased of freezing and thawing cycles during glacial phases (Sanchez et al., 2010; Lebrouc et al., 2013; Hilger et al., 2021). These observations therefore suggest that the CdB Gorge results from a vertical fluvial incision process, and is later widened by glacial and postglacial processes related to climate phases.

5.3. Regional comparison of river incision rates in SW Alps and possible controlling factors: climate, fluvial regime and surface uplift

Several studies based on CRE dating have been carried out on gorges and valleys of the SW Alps (Saillard et al., 2014; Rolland et al., 2017; Petit et al., 2019; Figure 7). The comparison of fluvial incision at the scale of SW Alps from gorges formed in valleys with or without glacial influence shows the dominance of high and variable incision rates in formerly glaciated catchments, while catchments devoid of glacial influence have lower incision rates since the LGM. Indeed, glaciated areas accumulate topographic disequilibrium during glaciation (Brocard and van der Beek, 2006). Readjustments after glacial perturbations imply enhanced erosion by fluvial and hillslopes processes, especially during deglaciation (Norton et al., 2010; Fox et al., 2015). In catchments dominated by glaciers during the LGM and Younger Dryas in their higher part, the above authors determined incision rates ranging from

1 mm/yr to ≈8 mm/yr (Figure 7B), which they attributed to efficient fluvial incision. The most extreme values are restricted to the catchments higher altitude (>900m) and can be attributed to transient incision of late glacial morphologies after the Younger Dryas (Rolland et al., 2017). In formerly glaciated areas, the post-LGM incision might be controlled by climatic variations, through punctual post-glacial outbursts, and topographic readjustment through transient headward erosion. Therefore, these locally very high incision rates cannot be used to infer any long-term tendency.

Out of the influence of glaciers, the incision rates estimated for the Estéron River (Petit et al., 2019) and the Bès River (this study) are of ≈ 1.0 and 0.15 mm/yr respectively (Figure 7; Petit et al., 2019; this study). However, if we compare incision rates between the Vésubie, Estéron and Bès rivers after the last cold climatic event (i.e., the Younger Dryas), despite the fact that all three profiles are measured in a similar lithology and under comparable climatic settings, the mean incision rate of the Bès river (0.15 mm/yr) appears significantly lower than in the Vésubie (2.0 ± 0.1mm/yr), like for all catchments with glacial influence. In comparison to a catchment positioned in a similar glacier-free setting, the Esteron River (1.0 ± 0.1 mm/yr), the river incision rate value estimated for the Bès is still significantly lower.

Surface uplift, which is a combination of isostatic rebound, tectonic uplift and erosion, may also cause incision rate variability (e.g. Kirby and Whipple, 2012). Isostatic rebound, either induced by Quaternary erosion and LGM glacier retreat, has been shown to be insignificant in the SW Alps (Norton and Hampel, 2010; Champagnac et al., 2017; Sternai et al., 2019). Regarding the tectonic uplift component, cooling rates from Apatite Fission Track measurements in the external crystalline massif of the Argentera-Mercantour (Bogdanoff et al., 2000; Bigot-Cormier et al., 2006) lead to long-term exhumation rates of 1.1-1.4 mm/yr (rock uplift) over the last 10 Myr. Closer to our study area, Schwartz et al. (2017)

421 demonstrated by low-temperature thermochronometry that the Barles erosional half-window
422 area has been exhuming at a long-term rate of ≈ 0.7 mm/yr since 5 Ma. Recent studies using
423 GPS monitoring in the Alps (Walpersdorf et al., 2018; Sternai et al., 2019) evidence a
424 present-day surface uplift rate of 0.5 to 1 mm/yr in the highest parts of the Alpine massifs,
425 while GPS stations closer to our study area (La Javie and Moustiers-Sainte-Marie) have short-
426 term uplift rates of 0.025+/-0.9 and -0.41+/-0.58 mm/yr, respectively (Sternai et al., 2019).
427 Hence, the relatively high incision rates recorded in the Var catchment and tributaries
428 compared to the slow rates determined at the CdB gorge may reflect the east to west (i.e.
429 massifs highest parts to Alpine foreland) regional variability of both long-term and short-term
430 uplift rates. Nevertheless, in order to better discriminate the respective role of local catchment
431 dynamics (glacial or not) and uplift rates variability on fluvial incision process, further
432 constraints on incision rates are needed at the scale of SW Alps.

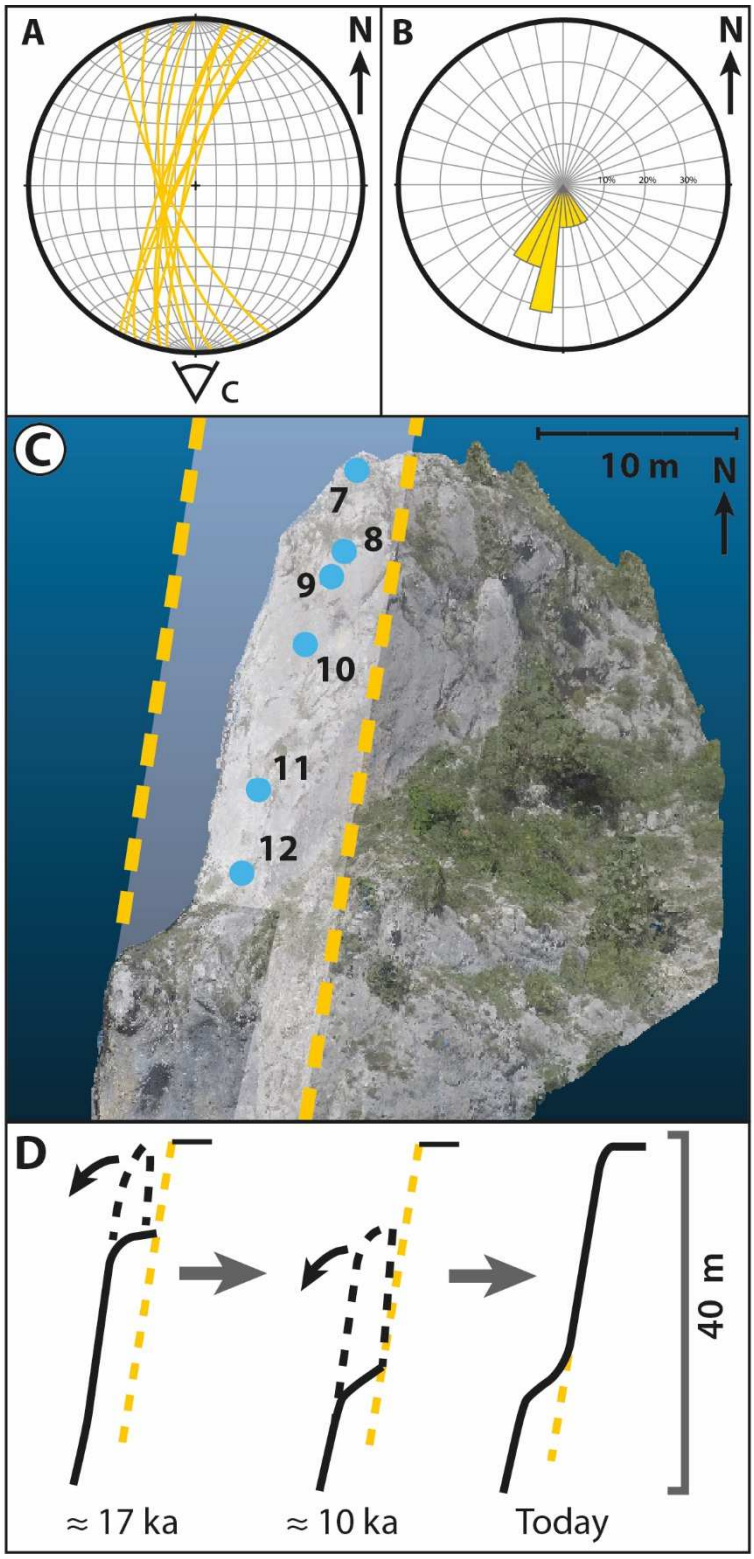

Figure 6. Geometrical characteristics of the rockfall domain in the middle part of the CdB Gorge profile. A-B, Dip and strike measurements of the sample profile upper part (calculated from the DEM) in a Wulff stereographic projection, lower hemisphere (A) and in a Rose diagram (B). C, Mean plane deduced from the DEM calculated strike and dip of the upper sampled surface (yellow dashed framed rectangle) and location of the rejuvenated samples (samples 7 to 12; blue dots). D. Interpretation of the rockfall process by toppling that

may have caused the rejuvenation of the sampled surface.

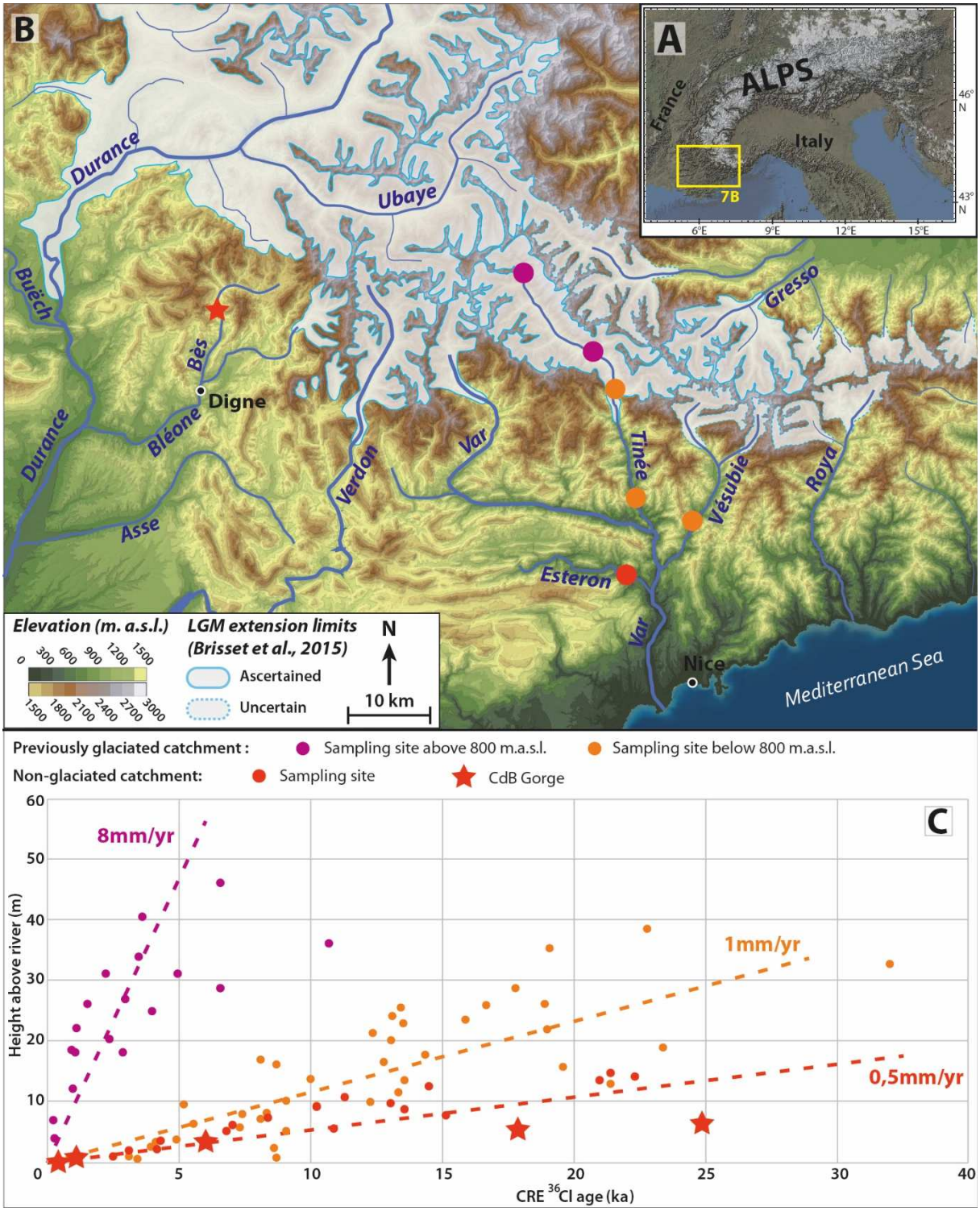

Figure 7. A, Location of study area in the European Alps. B, Location of the CdB Gorge from this study and previous ones (Saillard et al., 2014; Petit et al., 2019; Rolland et al., 2017) in the SW Alps set against the Last Glacial Maximum (LGM) extension limits (modified from Brisset et al., 2015). Note that the glaciated/non-glaciated specification refers to the glaciation of the catchment during the LGM, and not the sampling site itself. C, Comparison of incision rate determined by CRE dating from this study (red stars) and previous ones (Saillard

et al., 2014; Petit et al., 2019; Rolland et al., 2017). Note the increase of site specific incision rate according to their altitude and location in regard of the LGM extension limits.

5. CONCLUSION

We sampled and measured in situ-produced ^{36}Cl concentrations in twenty Jurassic limestone samples along an 80 m high sub-vertical and continuous profile of the V-shaped CdB Gorge (SW Alps) and in four samples collected at the top of the Jurassic limestone bar in which the CdB Gorge is incised. High-resolution DEM analysis and CRE ages show that the CdB Gorge was first dug by fluvial incision and subsequently widened by secondary gravitational processes. The top four samples are suggestive of a steady-state ^{36}Cl concentration that allows quantifying a denudation rate between 18 and 33 mm/kyr in the flatter upper, perfectly exposed surfaces on the shoulders of the gorge. CRE ages of the 10 m above riverbed profile allow quantifying a mean fluvial incision rate of 0.15 mm/yr over the last 25 ka, with an acceleration up to 2 mm/yr for the last 2 ka that can be linked to extreme flood events. The comparison of CRE dating results at the scale of SW Alps shows that the fluvial incision of Bès River is significantly lower than in other basins, which is ascribed to its frontal position in the Alps and glacier-free watershed during glacial phases. Moreover, CRE ages obtained in the middle part of the gorge are suggestive of two main rockfall events, which occurred ≈17 ka and ≈10 ka ago. These two events correspond to deglacial stages of the LGM and Younger Dryas, respectively, while their geometry suggests debuttressing along two recognized fracture families identified in the field. These data suggest the triggering of rockfalls in a warming climate during periglacial episodes. More sporadic rockfalls may explain age variability in the profile middle part. Based on this example, fluvial gorges in periglacial settings could be efficiently shaped by rockfalls during deglaciation periods, once fluvial incision has exposed the walls.

ACKNOWLEDGMENTS

This study has been supported and funded by the French Geological Survey (Bureau de

Recherches Géologiques et Minières; BRGM) through the national program “Référentiel Géologique de France” (RGF-Alpes), the AO7 OSUG@2020 (ANR10 LABX56) and by the CNRS-INSU SYSTER Program. The ^{36}Cl measurements were performed at the ASTER AMS national facility (CEREGE, Aix en Provence) which is supported by the INSU/CNRS, the ANR through the "Projets thématiques d’excellence" program for the "Equipements d’excellence" ASTER-CEREGE action and IRD. Fruitful discussions with Ludovic Ravanel benefited the interpretation of the results. The authors are grateful to Myette Guiomar from the Réserve naturelle nationale Géologique de Haute-Provence. The authors warmly thank Francis Coeur (GeoThermoChronology Platform, ISTerre) for the technical support. Magali Bonnefoy is thanked for her help in the sample preparation. We are grateful to two anonymous reviewers and to Editor Markus Stoffel for their insightful comments.

REFERENCES

Adams J., 1985. Large-scale tectonic geomorphology of the Southern Alps, New Zealand. In: Morisawa M., Hack J.T., Eds., Tectonic Geomorphology. Allen and Unwin, Boston, 105-128.

Arnold M., Merchel S., Bourlès D.L., Braucher R., Benedetti L., Finkel R.C., Aumaître G., Gottdang A. and Klein M., 2010. The French accelerator mass spectrometry facility ASTER: improved performance and developments. Nuclear Instruments and Methods in Physics Research, B 268, 1954–1959.

Bacon S.N., McDonald E.V., Caldwell T.G. and Dalldorf G.K., 2009. Timing and distribution of alluvial fan sedimentation in response to strengthening of late Holocene ENSO variability in the Sonoran Desert, southwestern Arizona, USA. Quaternary Res., 73, 425-438.

Balco G., Stone J.O., Lifton N.A. and Dunai T.J., 2008. A complete and easily accesible means of caltulating surfaces exposure ages or erosion rates from ^{10}Be and ^{26}Al

497 measurements. Quat. Geochronol., 3, 174-195.
498 Bigot-Cormier, Sosson M., Poupeau G., Stéphan J.-F. and Labrin E., 2006. The denudation
499 history of the Argentera Alpine External Crystalline Massif (Western Alps, France-
500 Italy): an overview from the analysis of fision tracks in apatites and zircons.
501 Geodinamica Acta, 19, 6, 455-473.
502 Bogdanoff S., Michard A., Mansour M. and Poupeau G., 2000. Apatite fission track analysis
503 in the Argentera massif: evidence of contrasting denudation rates in the External
504 Crystalline Massifs of the Western Alps. Terra Nova, 12, 117-125.
505 Braucher R., Merchel S., Borgomano J. and Bourlès D.L., 2011. Production of cosmogenic
506 radionuclides at great depth : a multi element approach. Earth Planet. Sci. Lett., 309, 1-9.
507 Braucher R., Keddadouche K., Aumaître G., Bourlès D.L., Arnold M., Pivot S., Baroni M.,
508 Scharf A., Rugel G. and Bard E., 2018. Chlorine measurements at the 5 MV French
509 AMS national facility ASTER: associated external uncertainties and comparability with
510 the 6MV DREAMS facility. Nuclear Inst, and Methods in Physics Research, B 420, 40–
511 45.
512 Brisset E., Guiter F., Miramont C., Revel M., Anthony E.J. , Belhon C., Arnaud F., Malet E.
513 and de Beaulieu J.-L., 2015. Lateglacial/Holocene environmental changes in the
514 Mediterranean Alps inferred from lacustrine sediments. Quaternary Sci. Rev., 110, 49-
515 71.
516 Brocard G.Y., Van Der Beek P., Bourlès D., Siame L. and Mugnier J.-L., 2003. Long-term
517 fluvial incision rate and postglacial river relaxation time in the French Western Alps
518 from ^{10}Be dating of alluvial terraces with assessment of inheritance, soil developpement
519 and wind ablations effects. Earth Planet. Sci. Lett., 209, 197-214
520 Brocard G. and van der Beek P., 2006. fluence of incision rate, rock strength, and bedload
521 supply on bedrock river gradients and valley-flat widths: Field-based evidence and

522 calibrations from western Alpine rivers (southeast France). Geological Society of
523 America, 398, 101-126.
524 Brocklehurst S.H. and Whipple K.X., 2002. Glacial erosion and relief production in the
525 Eastern Sierra Nevada, California. Geomorphology, 42, 1-24.
526 Champagnac, J.D., Molnar P., Andersion R.S., Sue C. and Delacou B., 2007. Quaternary
527 erosion-induced isostatic rebound in the western Alps. Geol. Soc. Am. Bull., 35, 3, 195-
528 198.
529 Champagnac J.D., van der Beek P., Diraison G. and Dauphin S., 2008. Flexural isostatic
530 response of the Alps to increased Quaternary erosion recorded by foreland basin
531 remnants, SE France. Terra Nova, 20, 213-220.
532 Clark P.U., Dyke A.S., Shakum J.D., Carlson A.E., Clark J., Wohlfarth B., Mitrovica J.X.,
533 Hostetler S.W. and McCabe A.M., 2009. The Last Glacial Maximum. Science, 325, 710-
534 714.
535 Codilean A.T., 2006. Calculation of the cosmogenic nuclide production topographic shielding
536 sclaning factor for large areas using DEMs. Earth Surf. Proc. Land., 31, 6, 785-794.
537 Darnault R., Rolland R., Rolland Y., Bourlès D., Revel M., Sanchez G. and Bouissou S.,
538 2012. Timing of the last deglaciation revealed by receding glaciers at the Alpine-scale:
539 impact on mountain geomorphology. Quaternary Sci. Rev., 3, 127-142.
540 Delacou B., Sue C., Champagnac J.-D. and Burkhard M., 2004. Present-say geodynamics in
541 the bend of the western and central Alps as constrained by earthquake analysis. Geophys.
542 J. Int., 158, 753-774.
543 Dumont T., Schwartz S., Guillot S., Simon-Labric T., Tricart P. and Jourdan S., 2012.
544 Structural and sedimentary records of the Oligocene revolution in the Western Alpine
545 arc. J. Geodyn., 56-57, 18-38.
546 Dunne F., Elmore D. and Muzikar P., 1999. Scaling factors for the rates of production of

cosmogenic nuclides for geometric shielding and attenuation at depth on sloped surfaces. Geomorphology, 27, 3-11.

England P. and Molnar P., 1990. Surface uplift, uplift of rocks, and exhumation of rocks. Geology, 18, 1173-1177.

Fox M., Leith K., Bodin T., Balco G. and Shuster D.L., 2015. Rate of fluvial incision in the Central Alps constrained throught joint inversion of detrital 10Be and thermochronometric data. Earth and Planetary Science Letters, 411, 27-36.

Godard V., Ollivier V., Bellier O., Miramont C., Shabanian E., Fleury J., Benedetti L., Guillou V. and ASTER Team, 2016. Weathering-limited hillslope evolution in carbonate landscapes. Earth Planet. Sci. Lett., 446, 10-20.

Godard V., Hippolyte J.-C., Cushing E., Espurt N., Fleury J., Bellier O., Ollivier V. and ASTER Team, 2020. Hillslope denudation and morphologic response across a rock uplift gradient. Earth Surf. Dynam., 8, 221–243.

Gosse J. and Phillips F., 2001. Terrestrial in situ cosmogenic nuclides: Theory and application. Quaternary Sci. Rev., 20, 1475-1560.

Hilger P., Hermanns R. L., Czekirda J., Myhra K. S., Gosse J.C. and Etzelmüller B., 2021. Permafrost as a first order control on long-term rock-slope deformation in (Sub-) Arctic Norway. Quaternary Science Reviews, 251, 106718.

Hippolyte J.-C. and Dumont T., 2000. Identification of Quaternary thrusts folds and faults in a low seismicity area: examples in the Southern Alps (France). Terra Nova, 12, 156-162.

Kirby E. and Whipple K.X., 2012. Expression of active tectonics in erosional landscapes. J. Struct. Geol., 44, 54-75.

Korup O. and Schlunegger F., 2007. Bedrock landsliding, river incision, and transience of geomorphic hillslope-channel coupling: Evidence from inner gorges in the Swiss Alps. J. Geophys. Res., 112, F03027.

572 Lal D., 1991. Cosmic ray labeling of erosion surfaces: in situ nuclide production rates and
573 erosion models. Earth Planet. Sci. Lett., 104, 424-439.
574 Lavé J. and Avouac J.P., 2001. Fluvial incision and tectonic uplift across the Himalayas of
575 central Nepal. J. Geophys. Res., 106, B1, 25 561-25 593.
576 Lebrouc V., Schwartz S., Baillet L., Jongmans D. and Gamond J.F., 2013. Permafrost
577 extension modeling in a rock slope since the Last Glacial Maximum : application to the
578 large Séchilienne landslide (French Alps). Geomorphology, 198, 189-200.
579 Li Y.-K., 2013. Determining topographic shielding from digital elevation models for
580 cosmogenic nuclide analysis : a GIS approach and field validation. J. Mt. Sci., 10, 3,
581 355-362.
582 Li Y.-K., 2018. Determining topographic shielding from digital elevation models for
583 cosmogenic nuclide analysis: a GIS model for discrete sample sites. J. Mt. Sci., 15, 5
584 939-947.
585 Merchel S., Bremser W., Alfimov V., Arnold M., Aumaître G., Benedetti L., Bourlès D.L.,
586 Caffee M., Fifield L.K., Finkel R.C., Freeman S. P. H. T., Martschini M., Matsushi Y.,
587 Rood D.H., Sasa K., Steier P.,Takahashi T.,Tamari M., Tims S.G., Tosaki Y., Wilcken
588 K.M. and Xu S., 2011. Ultra-trace analysis of 36Cl by accelerator mass spectrometry: an
589 interlaboratory study , Anal. Bioanal. Chem., 400, 3125-3132.
590 Montgomery D.R., 2002. Valley formation by fluvial and glacial erosion. Geology, 30, 1047-
591 1050.
592 Montgomery D. R. and Korup O., 2010. Preservation of inner gorges through repeated Alpine
593 glaciations. Nat. Geosci., 4, 62-67.
594 Nocquet J.-M., Sue C., Walpersdorf A., Tran T., Lenôtre N., Vernant P., Cushing M., Jouanne
595 F., Masson F., Baize S., Chéry J. and van der Beek P. A., 2016. Present-day uplift of the
596 western Alps. Sci. Rep., 6, 28404.

Norton K.P. and Vanacker V., 2009. Effects of terrain smoothing on topographic shielding correction factors for cosmogenic nuclide-derived estimates of basin-averaged denudation rates. Earth Surf. Proc. Land., 34, 145-154.

Norton K.P., Abbühl L.M. and Schlunegger F., 2010. Glacial conditioning as an erosional driving force in the Cenral Alps. Geology, 38, 7, 655-658.

Norton K.P. and Hampel A., 2010. Postglacial rebound promotes glacial re-advances – a case study from the European Alps. Terra Nova, 22, 297-302.

Ouimet W.B., Whipple K.X., Crosby B.T., Johnson J.P. and Schildgen T.F., 2008. Epigenetic gorges in fluvial landscapes. Earth Surf. Proc. Land., 33, 13, 1993-2009.

Pan B., Burbank D.W., Wang Y., Wu G., Li J. and Guan Q., 2003. A 900 k.y. Record of strath terrace formation during glacial-interglacial transitions in northwest China. Geology, 31, 957-960.

Pazzaglia F. J., Gardner T. W. and Merritts D. J., 1998. Bedrock fluvial incision and longitudinal profile development over geological time scales determined by fluvial terraces. In: Wohl, E., Tinkler, K. (Eds.), Bedrock Channels. American Geophysical Union. Geophysical Monograph Series 107, Washington, 207–235.

Petit C., Rolland Y., Braucher R., Bourlès D., Guillou V. and Petitperrin V., 2019. River incision and migration deduced from ^{36}Cl cosmic-ray exposure durations: The Clue de la Cerise gorge in southern French Alps. Geomorphology, 330, 81-88

Petit, C., Goren, L., Rolland, Y., Bourlès, D., Braucher, R., Saillard, M. and Cassol, D., 2017. Recent, climate-driven river incision rate fluctuations in the Mercantour crystalline massif, southern French Alps. Quaternary Sci. Rev., 165, 73-87.

Pratt B., Burbank D.W., Heimsath A. and Ojha T., 2002. Impulsive alluviation during early Holocene strengthened monsoons, central Nepal Himalaya. Geology, 30, 10, 911-914.

Ravanel L., Allignol F., Deline P., Gruber S. and Ravello M., 2010. Rockfalls in the Mont

622 Blanc Massif in 2007 and 2008. Landslides, 7, 4, 493-501.
623 Rolland Y., Petit C., Saillard M., Braucher R., Bourlès D., Darnault R., Cassol D. and ASTER
624 Team, 2017. Inner gorges incision history: A proxy for deglaciation ? Insights from
625 Cosmic Ray Exposure dating (^{10}Be and ^{36}Cl) of river-polished surfaces (Tinée River, SW
626 Alps, France). Earth Planet. Sci. Lett., 457, 271-281.
627 Ryb U., Matmon A., Erel Y., Haviv I., Katz A., Starinsky A., Angert A. and ASTER Team,
628 2014a. Controls on denudation rates in tectonically stable Mediterranean carbonate
629 terrain. The Geol. Soc. Am. Bull. Bulletin, 126, 553-568.
630 Ryb U., Matmon A., Erel Y., Haviv I., Benedetti L. and Hidy A.J., 2014b. Styles and rates of
631 long-term denudation in carbonate terrains under a Mediterranean to hyper-arid climatic
632 gradient. Earth Planet. Sci. Lett., 406, 142-152.
633 Sadier B., Delannoy J.-J., Benedetti L., Bourlès D.L., Jaillet S., Geneste J.-M., Lebatard A.-E.
634 and Arnold M., 2012. Further constraints on the Chauvet cave artwork elaboration.
635 Proceedings of the National Academy of Sciences of the United States of America, 109,
636 8002-8006.
637 Saillard M., Petit C., Rolland Y., Braucher R., Bourlès D. L., Zerathe S., Revel M. and
638 Jourdon A., 2014. Late Quaternary incision rates in the Vésubie catchment area
639 (Southern French Alps) from in situ-produced ^{36}CI cosmogenic nuclide dating: Tectonic
640 and climatic implications. J. Geophys. Res. Earth Surface, 119, 1121-1135.
641 Sanchez G., Rolland Y., Corsini M., Braucher R., Bourlès D., Arnold M. and Aumaître G.,
642 2010. Relationships between tectonics, slope instability and climate change: Cosmic Ray
643 exposure dating of active faults, landslides and glacial surfaces in the SW Alps.
644 Geomorphology, 107, 1-2, 1-13.
645 Schaller M., Hovius N., Willett S.D., Ivy-Ochs S., Synal H.-A. and Chen M.-C., 2005. Fluvial
646 bedrock incision in the active mountain belt of Taiwan from in situ-produced

647 cosmogenic nuclides. Earth Surf. Proc. Land., 30, 955-971.
648 Schimmelpfennig I., Benedetti L., Finkel R., Pik R., Blard P.-H., Bourlès D.L., Burnard P. et
649 Williams A., 2009. Source of in situ ^{36}Cl in basaltics rocks. Implication for calibration of
650 production rates. Quat. Geochronol., 4, 441-461.
651 Schwartz S., Gautheron C., Audin L., Dumont T., Nomade J., Barbarand J., Pinna-Jamme R.
652 and van der Beek P., 2017. Foreland exhumation controlled by crustal thickening in the
653 Western Alps. Geology, 45, 2, 139-142.
654 Serpelloni E., Faccenna C., Spada G., Dong D. and Williams S. D. P., 2013. Vertical GPS
655 ground motion rates in the Euro-Mediterranean region: New evidence of velocity
656 gradients at different spatial scales along the Nubia-Eurasia plate boundary. J. Geophys.
657 Res.: Solid Earth, 118, 6003-6024.
658 Sternai P., Sue C., Husson L., Serpelloni E., Becker T.W., Willet S.D., Faccenna C., Giulio
659 A.D., Spada G., Jolivet L., Valla P., Petit C., Nocquet J.-M., Walpersdorf A. and
660 Castelletort S., 2019. Present-day uplift of the European Alps: Evaluating mechanisms
661 and models of their relative contributions. Earth-Sci. Rev., 190, 589-604.
662 Stone J.O., 2000. Air pressure and cosmogenic isotope production. J. Geophys. Res.: Solid
663 Earth, 105, 23 753-23 759.
664 Sue C., Delacou B., Champagnac J.-D., Allanic C. and Burkhard., 2007. Aseismic
665 deformation in the Alps: GPS vs. seismic strain quantification. Terra Nova, 1, 182-188.
666 Thomas F., Godard V., Bellier O., Shabanian E., Ollivier V., Benedetti L., Rizza M., Espurt
667 N., Guillou V., Hollender F., Molliex S. and ASTER Team, 2017. Morphological
668 controls on the dynamics of carbonate landscapes under a mediterranean climate. Terra
669 Nova, 29, 3, 173-182.
670 Valla P.G., van der Beek P.A. and Carcaillet J., 2010. Dating bedrock gorge incision in the
671 French Western Alps (Ecrin-Pelvoux massif) using cosmogenic ^{10}Be. Terra Nova, 22,

672 18-25.
673 Valla P.G., Shuster D.L. and van der Beek P.A., 2011. Significant increase in relief of the
674 European Alps during mid-Pleistocene glaciations. Nat. Geosci., 4, 688–692.
675 Van der Woerd J., Tapponnier P., Ryerson F.J., Meriaux A.-S., Meyer B., Gaudemer Y.,
676 Finkel R.C., Caffee M.W., Zhao G. and Xu Z., 2002. Uniform postglacial slip-rate along
677 the central 600 km of the Kunlun Fault (Tibet), from ^{26}Al, ^{10}Be, and ^{14}C dating of riser
678 offsets, and climatic origin of the regional morphology. Geophys. J. Int., 148, 356-388.
679 Vasquez-Tarrio D., Borgniet L., Liébault F. and Recking A., 2017. Using UAS optical
680 imagery and SfM photogrammetry to characterize the surface grain size of gravel bars in
681 a braided river (Vénéon River, French Alps). Geomorphology, 285, 94-105.
682 Walpersdorf A., Pinget L., Vernant O., Sue C., Deprez A. and RENAG team, 2018. Does
683 long-term GPS in the Western Alps finally confirm earthquake mechanisms? Tectonics,
684 37, 3721-3737.
685 Whipple K.X., Kirby E. and Brocklehurst S.H., 1999. Geomorphic limits to climate-induced
686 increases in topographic relief. Nature, 401, 39-43.
687 Wobus C., Whipple K.X., Kirby E., Snyder N., Johnson J., Spa opolou K., Crosby B. and
688 Sheehan D., 2006. Tectonics from topography: procedures, promise, and pitfalls. In:
689 Willett S.D., Hovius N., Brandon M.T., Fisher D.M., Eds., Tectonics, Climate, and
690 Landscape Evolution. Geol. Soc. Am. Bull. Special Paper, 398, 55-74.
691 Zerathe S., Lebourg T., Braucher R. and Bourlès D., 2014. Mid-Holocene cluster of larger-
692 scale landslides revealed in the Southwestern Alps by ^{36}Cl dating. Insight on an Alpine-
693 Scale landslide activity. Quaternary Sci. Rev., 90, 106-127.